Available online at www.sciencedirect.com
ScienceDirect
Electrochimica Acta 53 (2007) 752–757
ELECTROCHIMICA Acta
www.elsevier.com/locate/electacta

Interfacial synthesis of porous MnO_2 and its application in electrochemical capacitor

Xin-hui Yang, Yong-gang Wang, Huan-ming Xiong, Yong-yao Xia *

Chemistry Department and Shanghai Key Laboratory of Molecular Catalysis and Innovative Materials, Fudan University, Shanghai 200433, China

Received 30 March 2007; received in revised form 21 July 2007; accepted 22 July 2007
Available online 26 July 2007

Abstract

In this paper, the porous manganese dioxide ($MnO_{2)}$ was prepared by an interfacial reaction of potassium permanganate in water/ferrocene in chloroform. The surface area and pore distribution of MnO_2 can be controlled by simply adjusting the reaction time and the content of surfactant in the aqueous phase. The electrochemical performance of the prepared MnO_2 was evaluated as an electrode material for supercapacitors by the means of cyclic voltammetry and galvanostatic charge–discharge tests. Electrochemical tests results indicated that the pore size plays an important role at high charge–discharge rate, the sample with a large pore size shows a better rate capability, while the sample with a small pore size but large surface area delivers a large capacitance at low current rate.

Keywords: Porous MnO_2; Interfacial synthesis; Supercapacitor

1. Introduction

In recent years, the growing interest in supercapacitors has been stimulated by their potential application as electrical storage devices operating in parallel with the battery in an electric vehicle to transiently provide high power [1,2]. Electrochemical supercapacitors (ECs) fill the gap between batteries and conventional capacitors in terms of their specific energy and specific power [3–5]. Supercapacitors have been used as small-scale energy storage devices in stationary electronics, such as memory back-up devices and solar batteries with semi-permanent charge–discharge cycle life [6,7].

Depending on the charge storage mechanism, ECs are categorized as electrochemical double layer capacitor (EDLC) and pseudocapacitors. In electrochemical double layer capacitors, the charge is separated across the interface between the electrode and the electrolyte. Various carbonaceous materials ranging from amorphous carbons to carbon nanotubes have been used as electrode materials in EDLCs. In the case of pseudocapacitors, the Faradic charge transfer occurs between electrolyte and electrode. Various noble and transition metal oxides such as RuO_2, IrO_2, NiO_2, CoO_x, SnO_2, and MnO_2 were used as electrode materials [8–12]. Among these materials, amorphous hydrated ruthenium oxide exhibits ideal pseudocapacitive behavior, remarkably high specific capacitance as high as 700–1000 F/g [8], and excellent reversibility. However, the high cost and the toxicity to environment have limited its practical application. Therefore, some cheap and environmentally friendly materials have got more and more attention. MnO_2 is the most promising candidate because of its low cost and environmentally benign nature [13].

Manganese oxides as pseudocapacitor electrode materials were synthesized using different technique such as simple reduction, coprecipitation, thermal decomposition and sol–gel processes, etc. Also, various thin film electrodes of MnO_2 were synthesized via electrochemical and chemical routes [14–16]. Organic-aqueous interfacial synthesis is an alternative useful approach to conventional homogeneous synthesis. A liquid/liquid interface offers potential for the chemical manipulation of nanoparticles. At a liquid/liquid interface, the particles are highly mobile and rapidly achieve an equilibrium assembly. Interfaces between immiscible fluids have been shown to be ideal for the assembly of nanometer-sized colloidal particles [17]. For nanoparticles, thermal energy, which causes spatial fluctu-

* Corresponding author. Tel.: +86 21 55664177; fax: +86 21 55664177.
E-mail address: yyxia@fudan.edu.cn (Y.-y. Xia).

0013-4686/$ – see front matter © 2007 Elsevier Ltd. All rights reserved.
doi:10.1016/j.electacta.2007.07.043

ations of the particles, is comparable to the interfacial energy. This energy balance results in a weak interfacial aggregation of nanoparticles. The liquid/liquid interface provide easy access to the nanoparticles for their self-assembly by the reaction of the attached ligands. It has been employed to obtain nanoparticles such as Au, Ag, Pd, Cu, CuS, CuSe, CuO and $Cu(OH)_2$ in the literatures [18–24].

In this paper, we for the first time report the synthesis of porous MnO_2 employed organic/aqueous interface. The size of MnO_2 was achieved by simply tuning the concentration of the surfactant in the aqueous phase. The effects of the particle size, pore size, and the surface area on the capacitance performance of the MnO_2 were studied extensively.

2. Experimental

2.1. Synthesis and characterization of MnO_2

MnO_2 were prepared at the interface between organic phase and aqueous phase at room temperature. The aqueous phase contains a mixture of potassium permanganate ($KMnO_4$) and sodium dodecylsulfate (SDS) which serves as surfactant in water. The concentration $KMnO_4$ was 0.01 M and the SDS concentration is 3, 8, 16, 40, 80, 120, 160 and 320 mM, respectively. 25 ml above solution was added on the 25 ml, 0.03 M ferrocene/$CHCl_3$ solution. A static organic/aqueous interface was formed. After a short introduction period, some puce products appeared at the interface. As the puce products were produced continuously, the color of the aqueous phase turned lighter and lighter until a puce precipitate layer was formed at the liquid/liquid interface. The organic phase was removed by the pipette in a given time varying from 3.5 to 24 h. The puce precipitates and the aqueous phase were collected and centrifuged at 6000 rpm for 6 min. The precipitates were settled down to the bottom of the container under centrifugation then washed with distilled water and ethanol repeatedly until the liquid phase was colorless after centrifugation. The product was dried at 70 °C in a vacuum for 10 h. The product prepared from the different SDS contents mentioned above are denoted as sample A, B, C, D, E, F, G and H. The prepared MnO_2 was characterized by the X-ray diffraction (XRD, Bruker D8), scanning electronic microscope (SEM, Philip XL30) and BET surface area measurement (Micromeritics Tristar).

2.2. Electrochemical tests

The electrode of MnO_2 was prepared according to the following steps. The mixture containing 80 wt.% MnO_2 and 15 wt.% acetylene black and 5 wt.% polytetrafluoroethylene (PTFE) was well mixed, and then was pressed onto nickel foam grid (1.2×10^7 Pa) that served as a current collector (surface is 1 cm^2). The typical mass load of electrode material is 5 mg. The used electrolyte was 0.5 M potassium sulfate. The electrochemical behavior of MnO_2 was characterized by cyclic voltammetry and charge–discharge tests. The experiments were carried out in a three-electrode glass cell. Platinum foil was used as a counter electrode, and SCE as a reference electrode. The electrochemical measurements were performed using a Solartron Instrument Model 1287 electrochemical interface controlled by a computer.

3. Results and discussion

3.1. Characterization of materials

A series of MnO_2 were prepared by the interfacial reaction of potassium permanganate ($KMnO_4$)/sodium dodecylsulfate (SDS)/ferrocene containing various concentration of SDS varying from 3, 8, 16, 40, 80, 120 and 160 to 320 mM. The schematic graph of the formation of MnO_2 can be described in Fig. 1. At the present of SDS, the micelles were formed and acted as colloid nanoreactors. The micelles containing permanganate salt arranged at the aqueous/organic interface, ferrocene molecule contacted the permanganate at the core of the micelles, redox took place at the interface and the MnO_2 particles were formed in the micelles. All samples show the very similar XRD patterns. Fig. 2 shows the selected XRD patterns of MnO_2 prepared at different concentrations of SDS, from 3, 80 to 320 mM (samples A, E and H). All three samples present broad XRD peaks, indicating the amorphous nature.

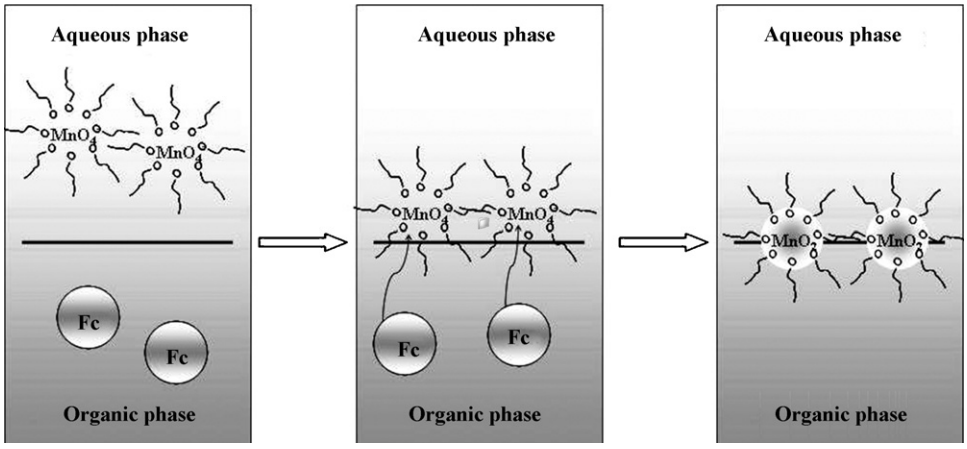

Fig. 1. Schematic graph of the formation of MnO_2 at interface of potassium permanganate in water/ferrocene in chloroform.

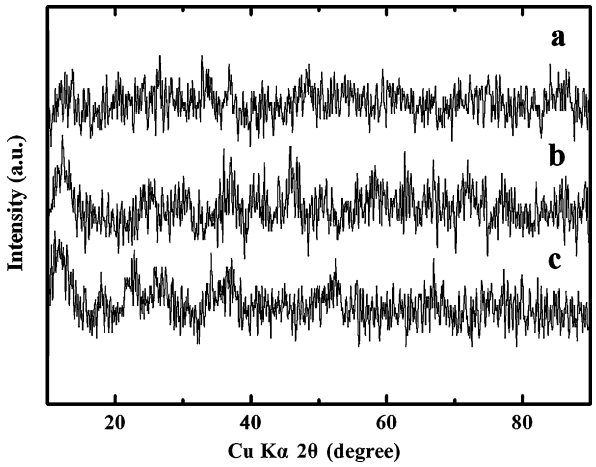

Fig. 2. X-ray diffraction patterns of MnO_2 synthesized at the interface between organic/aqueous interface for different concentrations of SDS in aqueous phase. (a) 3 mM (sample A); (b) 80 mM (sample E) and (c) 320 mM (sample H).

In order to optimize the reaction parameters, the reaction time is investigated. Fig. 3 gives the SEM image of the sample E prepared at the different times, 3.5, 4.5, 6.5 and 24 h, respectively. The particle size of MnO_2 increases with increasing of the reaction time. As demonstrated later, the sample prepared at 4.5 h delivers the highest specific capacitance of 260 F/g. The reaction time is fixed at 4.5 h. The effect of the added SDS concentration on the morphology was investigated. Fig. 4 presents the SEM image of the MnO_2. The images reveal the MnO_2 is aggregated spherical particle. The particle sizes decrease from 300 to 30 nm when the concentrations of SDS increase from 3 to 320 mM. The samples prepared in low concentration of SDS have much more compact morphologies. N_2 adsorption–desorption studies were performed to determine the specific surface area of the MnO_2 prepared at different concentrations of SDS. The BET surface area (Fig. 5) decreases gradually from 264 m^2/g of sample A to 173 m^2/g of sample H. The adsorption average pore diameter is 7.4, 13.1 and 16.7 nm for the samples A, E and H, respectively. This is the reason why sample A has the largest surface area even it has the largest particle size as the SEM images shown in Fig. 4. It is clear that the surface area mainly contributes from the pore in the MnO_2 particle. The detailed pore size distribution is presented in Fig. 6. Sample A has a narrow pore size distribution around 5 nm; sample E shows the pore size distribution with an average pore size of 5 and 15 nm, while sample H has a pore size around 5 and 30 nm. The amount of micelles increases and micelle size decreases when the concentration of surfactant SDS increases, thus leads to smaller particle size. On the other hand, the distance between the micelles increases when the concentrations of SDS increase because of the increasing charge repulsion. Therefore, the particle size depends on the micelle size while the pore size is associated with the distance between the micelles.

3.2. Electrochemical tests

Fig. 7 shows the CV curves of sample E at different scan rates from 2, 5, to 10 mV/s over the voltage range of 0.0–0.8 V versus SCE in 0.5 M K_2SO4 solution. The *Y*-axis of capacitance was calculated by the formula $C = i/v$ where C is the differential capacitance, i is the current density, v is the scan rate. As shown in Fig. 6, the typical quasi-rectangular curves indicate good EDLC behaviors. Moreover, the good rectangular sym-

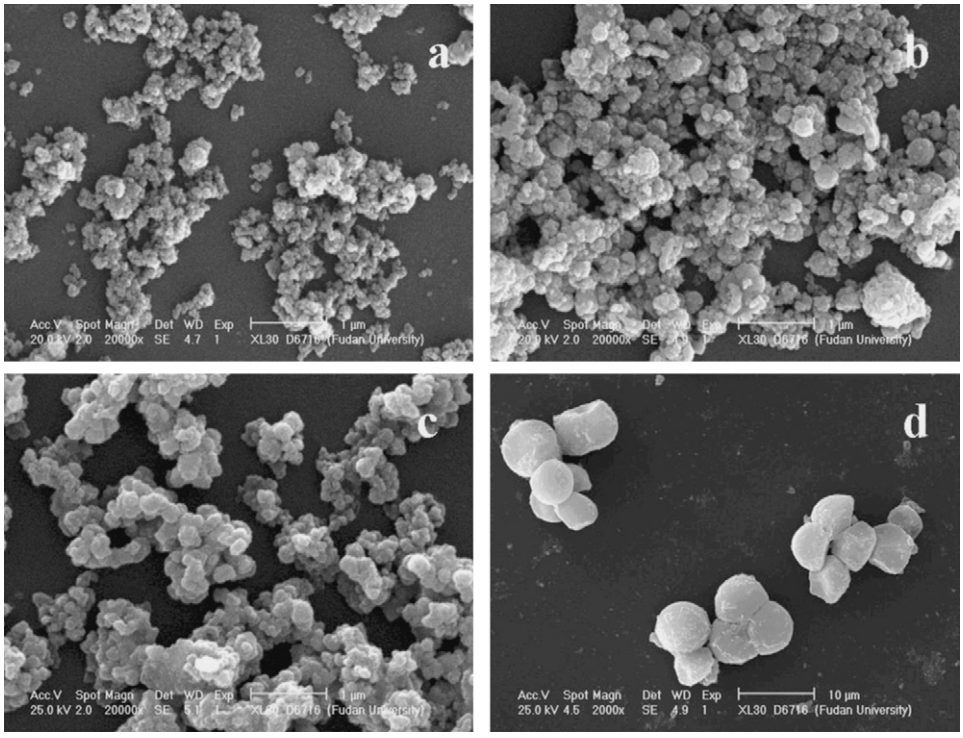

Fig. 3. SEM images of MnO_2 prepared at different reaction times: (a) 3.5 h; (b) 4.5 h; (c) 6.5 h; and (d) 24 h.

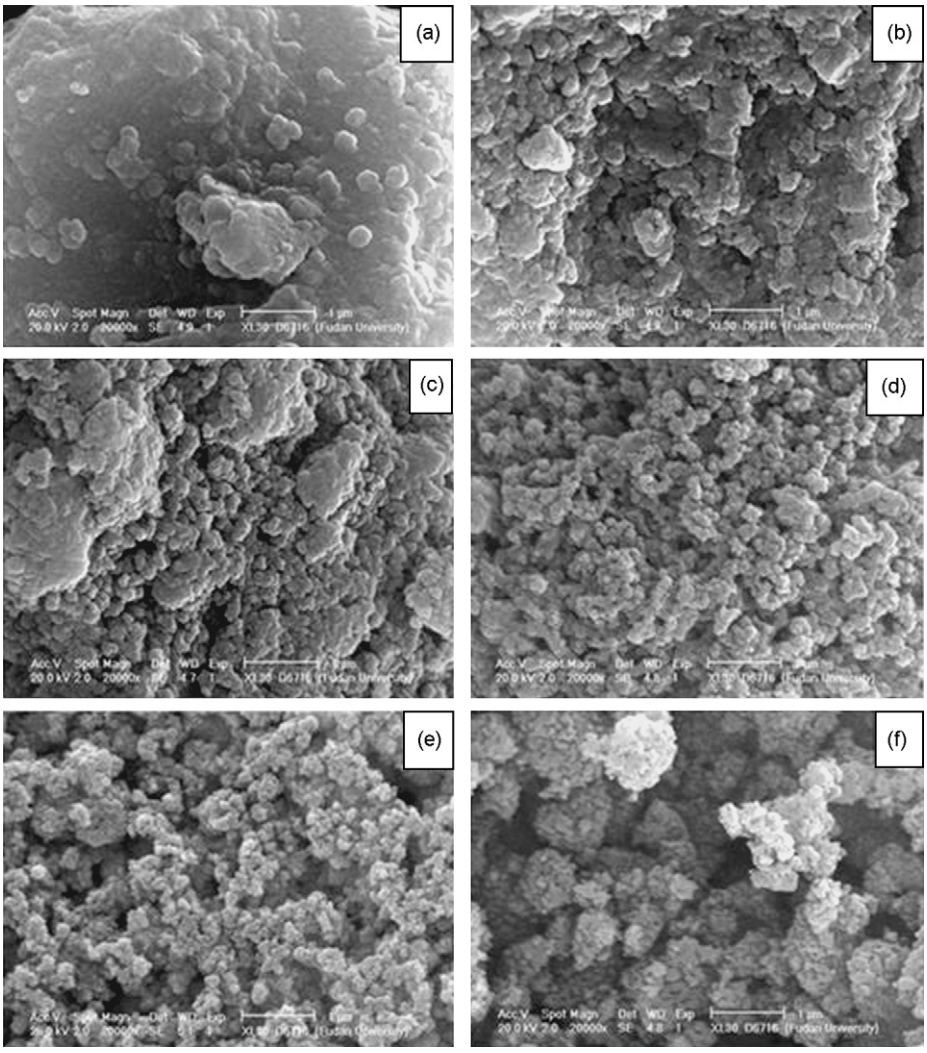

Fig. 4. SEM of images of the MnO_2 materials obtained at room temperature and 4.5 h. Panels a, b, c, d, e, f correspond to the samples synthesized from 3, 8, 40, 80, 160 and 320 mM SDS in aqueous phase, respectively.

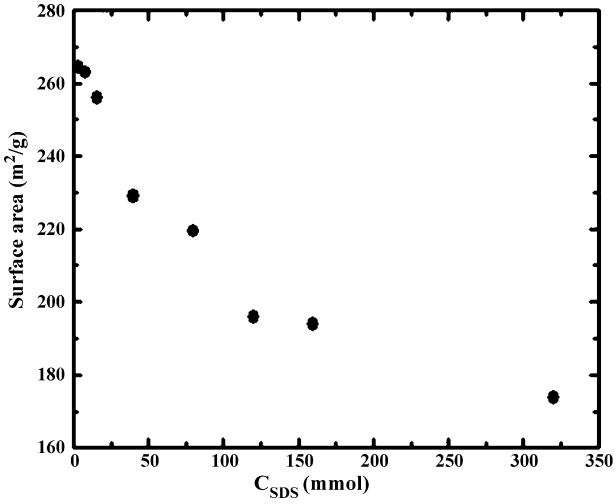

Fig. 5. Surface areas of MnO_2 materials synthesized at the presence of 3, 8, 16, 40, 80, 120, 160 and 320 mM SDS in the aqueous phase.

metry of CV curves can be surely maintained in the 0–0.8 V region when the scan rate is increased from 2 to 10 mV/s, which indicates the excellent capacitive ability of MnO_2 even at high current density.

The galvanostatic charge–discharge behavior of MnO_2 was investigated within potential range 0.0–0.8 V versus SCE in 0.5 M K_2SO4 solution at different currents. The current density varied from 40 to 0.5 mA/cm^2. The specific capacitance (C_m) can be calculated as follows:

$$C_m = \frac{C}{m} = \frac{It}{\Delta Vm}$$

where I is the current of charge–discharge, t the time of discharge, ΔV is 0.8 V, and m the mass of active materials in the working electrode. Table 1 shows the specific capacitance of the eight samples at different charge–discharge current densities.

Broadly speaking, the specific capacitance increases with the decrease of current density for all eight samples, while the increase tendency varies from sample to sample. The difference can be more clearly observed in Fig. 8 for the three selected samples, samples A, E and H. For sample A, the capacitance

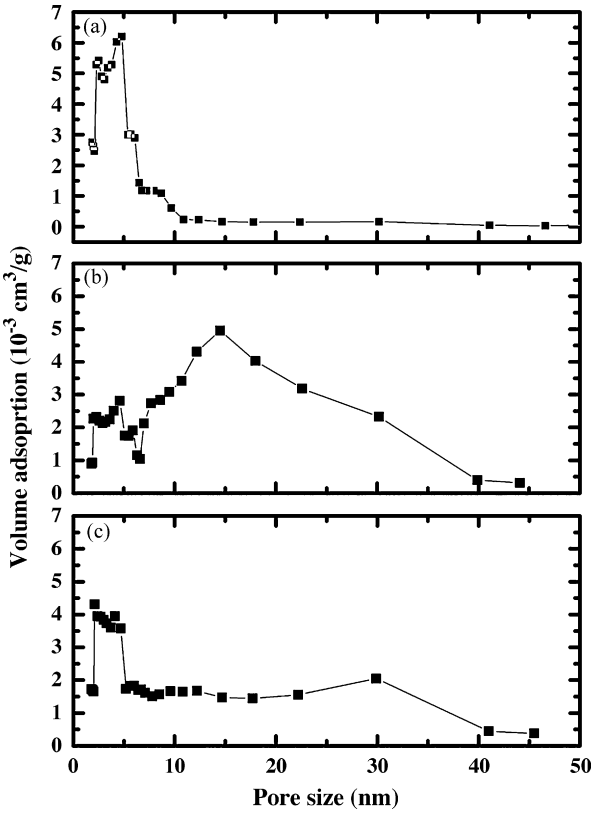

Fig. 6. Pore size distribution (a) for sample A, (b) for sample E and (c) for sample H.

rapidly decrease from 229 to 151 F/g when the current density increase from 0.5 to 5 mA/cm^2, then decrease slowly when the current rate further increases. The capacitance at 40 mA/cm^2 is only 98 F/g, only 40% of the capacitance at 0.5 mA/cm^2. Sample E shows the highest capacitance among all eight samples. The capacitance decreases slowly from 261 to 151 F/g when the current rate increase from 0.5 to 40 mA/cm^2; for sample H, the capacitance decrease very slowly from 219 to 200 F/g when the current rate increases from 0.5 to 5 mA/cm^2. It keeps 80% of the capacitance at 0.5 mA/cm^2, even at 40 mA/cm^2.

Table 1
Specific capacitance of MnO_2 prepared at different concentrations of SDS in different current densities

Current density (mA/cm^2)	Specific capacitance (F/g)							
	A	B	C	D	E	F	G	H
40	98	122	125	146	155	155	158	176
30	108	132	135	150	165	165	168	184
20	129	134	148	163	184	176	182	184
10	134	139	150	184	196	193	191	189
8	141	146	151	198	225	205	195	193
5	151	157	159	201	240	215	202	200
2	182	178	184	216	252	236	221	215
1	210	222	238	238	256	255	226	216
0.5	229	245	241	240	261	256	228	219

Sample H behaves the best rate capability among eight samples.

It is easy to be envisaged that difference in the capacitance behavior is associated with the pore size and its distribution. There have been two mechanisms proposed for the charge storage in MnO_2-based electrodes. The first one is base on the concept of intercalation of H^+ or alkali metal cations such as K^+ in the electrode during reduction and deintercalation upon oxidation [16,25].

$$MnO_2 + H^+ + e^- \rightleftharpoons MnOOH$$

or

$$MnO^2 + C^+ + e^- \rightleftharpoons MnOOC$$

$$(MnO_2)_{surface} + C^+ + e^- \rightleftharpoons (MnO_2{}^-C^+)_{surface}$$

The second mechanism is based on the surface adsorption of electrolyte cations (C^+) on MnO_2 [14].

Where $C^+ = Na^+$, K^+, Li^+. Despite of the inconsistent proposed mechanism, it has been demonstrated that the capacitance of the MnO_2 results from its surface reaction. Only a limited fraction of the MnO_2 is electrochemically active, the charge storage might only involve the surface atoms of the MnO_2 crystallites or a very thin layer. Therefore, the pseudocapacitance is critically

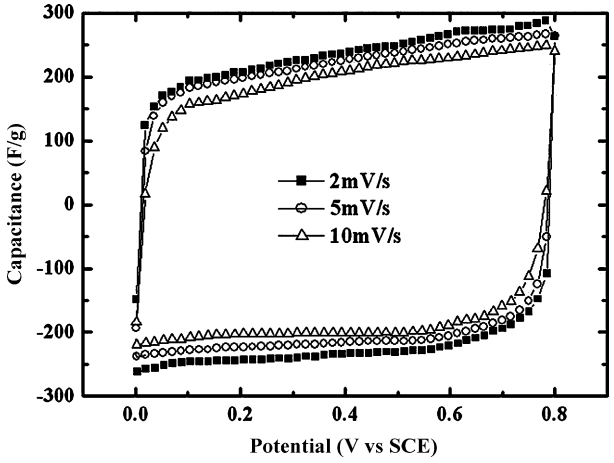

Fig. 7. CV curves of MnO_2 in 0.5 M K_2SO4 electrolyte at (a) 2 mV/s, (b) 5 mV/s and (c) 10 mV/s scan rate.

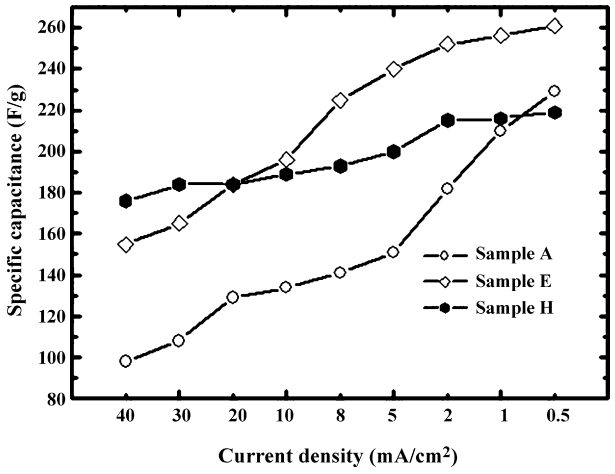

Fig. 8. Specific capacitance of samples A, E and H in different current densities.

Table 2
Pore volume proportions at the range of 7 nm below, 7–20 and 20 nm above, for samples A, E and H

Pore volume proportion (%)	Sample		
Pore size range (nm)	A	E	H
<7	70	20	10
7–20	20	55	30
>20	10	35	40

dependent on the effective surface area which is associated the particle size and pore distribution.

Generally, the specific capacitance increases with the increase of surface area. Sample A with the largest surface area has lower capacitance than sample H at high charge–discharge rate. Similar results of systems showing lower capacitance for a larger surface area material have been reported in the literature [26–29]. This indicates the specific capacitance does not depend on the surface area. Pore size distribution may be a deciding parameter in determining the specific capacitance. The pore volume proportions of samples A, E and H at different ranges are shown in Table 2. Sample A has 70% of the pore volume under 7 nm, compared to sample H with 10%. It leads to the sharp performance difference at high rate charge–discharge process because the pores under 7 nm are adverse for the fast intercalation and deintercalation of K^+. As the charge–discharge rate decreases to 0.5 mA/cm^2, sample A has larger capacitance than sample H because of larger surface area. Sample E has average distribution at the range of 3–40 nm. It keeps the active surface area and performs well at different charge–discharge rates. Sample H has the best rate capability for the contribution of 40% pore volume in the form of mesopores with diameter > 20 nm but poor performance for at low rate for the limitation of surface area.

Fig. 9 gives the charge–discharge cycling test of sample E synthesized at the present of 80 mM SDS at current density of 40 mA/cm^2 between 0 and 0.8 V versus SCE. As shown in Fig. 9, the MnO_2 exhibits good cycle profile, the capacitance slightly decreases 3% of initial capacity over 1300 cycles with a coulomb efficiency approximately 100%.

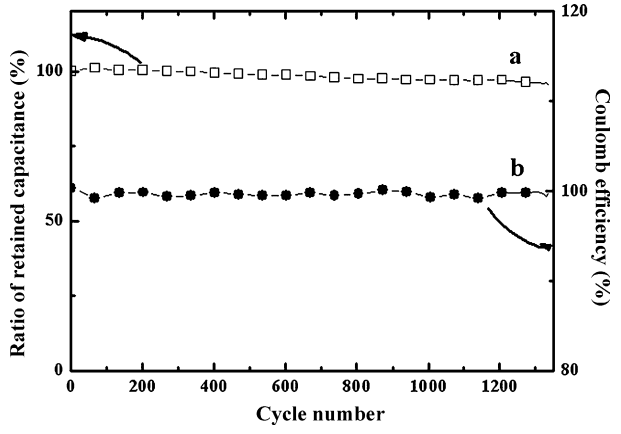

Fig. 9. Cycle performance of MnO_2 sample prepared in 80 mM SDS in aqueous solution, (a) ratio of retained capacitance and (b) coulomb efficiency.

4. Conclusion

In this paper, we successfully synthesized the porous MnO_2 with various pore sizes, varying from 5 to 30 nm by organic-aqueous interfacial method. The surface area and pore diameter of MnO_2 can be easily tuned by the content of SDS at aqueous phase. The pore diameter is the primary factor to affect the capacitance at high charge–discharge rate, while surface area becomes the primary factor at low charge–discharge rate. The MnO_2 synthesized under optimum conditions shows a capacitance of 261 F/g, and exhibits good cycle profile, keeping the 97% of initial capacity over 1300 cycles with a coulomb efficiency approximately 100%.

Acknowledgments

This work was partially supported by the National Natural Science Foundation of China (No. 20633040), the 863 program of China (No. 2006AA05Z218), and the State Key Basic Research Program of PRC (2007CB9700).

References

[1] B.E. Conway, J. Electrochem. Soc. 138 (1991) 1539.
[2] C. Arbizzani, M. Mastragostino, F. Soavi, J. Power Sources 100 (2001) 164.
[3] S.T. Mayer, R.W. Pekala, J.L. Kaschmitter, J. Electrochem. Soc. 140 (1993) 446.
[4] A. Yoshida, S. Nonaka, I. Aoki, A. Nishino, J. Power Sources 60 (1996) 213.
[5] Y. Kibi, T. Saito, M. Kurata, J. Tabuchi, A. Ochi, J. Power Sources 60 (1996) 225.
[6] Y.G. Wang, Y.Y. Xia, Electrochem. Commun. 7 (2005) 1138.
[7] M. Endo, T. Maeda, T. Takeda, Y.J. Kim, K. Koshiba, H. Hara, M.S. Dresselhaus, J. Electrochem. Soc. 148 (2001) A910.
[8] J.P. Zheng, P.J. Cygan, T.R. Jow, J. Electrochem. Soc. 142 (2001) 2699.
[9] K.C. Liu, M.A. Anderson, J. Electrochem. Soc. 143 (1996) 124.
[10] Y.S. Yoon, W.I. Cho, J.H. Lim, D.J. Choi, J. Power Sources 101 (2001) 126.
[11] B.E. Conway, V. Briss, J. Wojtowicz, J. Power Sources 66 (1997) 1.
[12] C. Lin, J. Ritter, B.N. Popov, J. Electrochem. Soc. 145 (1998) 4097.
[13] H.Y. Lee, S.W. King, Electrochem. Solid-State Lett. 4 (2001) A19.
[14] H.Y. Lee, J.B. Goodenough, J. Solid State Chem. 144 (1999) 220.
[15] H.Y. Lee, V. Manivannan, J.B. Goodenough, C. R. Chim. 2 (1999) 565.
[16] S. Pang, M.A. Anderson, T.W. Chapman, J. Electrochem. Soc. 147 (2000) 444.
[17] Y. Lin, H. Skaff, T. Emrick, A.D. Dinsmore, T.P. Russell, Nature 299 (2003) 226.
[18] L.L. Dai, R. Sharma, C.Y. Wu, Langmuir. 21 (2005) 2641.
[19] J.K. Sakata, A.D. Dwoskin, J.L. Vigorita, E.M. Spain, J. Phys. Chem. B 109 (2005) 138.
[20] F. Reincke, S.G. Hickey, W.K. Kegel, D. Vanmaekelbergh, Angew. Chem. 116 (2004) 464.
[21] A.W. Dryfe, A.O. Simm, B. Kralj, J. Am. Chem. Soc. 125 (2003) 13014.
[22] U.K. Gautam, M. Ghosh, C.N.R. Rao, Chem. Phys. Lett. 381 (2003) 1.
[23] U.K. Gautam, M. Ghosh, C.N.R. Rao, Langmuir 20 (2004) 10776.
[24] X.Y. Song, S.X. Sun, W.M. Zhang, H.Y. Yu, W.L. Fan, J. Phys. Chem. B 108 (2004) 5200.
[25] M. Toupin, T. Brousse, D. Belanger, Chem. Mater. 16 (2004) 3184.
[26] Y.U. Jeong, A. Manthiram, J. Electrochem. Soc. 149 (2002) A1419.
[27] R.N. Reddy, R.G. Reddy, J. Power Sources 124 (2003) 330.
[28] R.N. Reddy, R.G. Reddy, J. Power Sources 132 (2004) 315.
[29] V. Subramanian, H.W. Zhu, R. Vajtai, P.M. Ajayan, B.Q. Wei, J. Phys. Chem. B 109 (2005) 20207.